

Elastic/Plastic Indentation Damage in Ceramics: The Median/Radial Crack System

B. R. LAWN** and A. G. EVANS*

Department of Materials Science and Mineral Engineering, University of California, Berkeley, California 94720

D. B. MARSHALL*†

Department of Applied Physics, School of Physics, University of New South Wales, New South Wales 2033, Australia

A theory for describing the evolution of the median/radial crack system in the far field of sharp-indenter contacts is developed. Analysis is based on a model in which the complex elastic/plastic field beneath the indenter is resolved into elastic and residual components. The elastic component, being reversible, assumes a secondary role in the fracture process: although it does enhance downward (median) extension during the loading half-cycle, it suppresses surface (radial) extension to the extent that significant growth continues during unloading. The residual component accordingly provides the primary driving force for the crack configuration in the final stages of evolution, where the crack tends to near-half-penny geometry. On the hypothesis that the origin of the irreversible field lies in the accommodation of an expanding plastic hardness impression by the surrounding elastic matrix, the ensuing fracture mechanics relations for equilibrium crack growth are found to involve the ratio hardness-to-modulus as well as toughness. Observations of crack evolution in soda-lime glass provide a suitable calibration of indentation coefficients in these relations. The calibrated equations are then demonstrated to be capable of predicting the widely variable median and radial growth characteristics observed in other ceramic materials. The theory is shown to have a vital bearing on important practical areas of ceramics evaluation, including toughness and strength.

I. Introduction

THE fracture patterns generated by small-scale contact events relate strongly to the general mechanical behavior of ceramics. This is particularly true of contacts with "sharp" indenters, where elastic/plastic stress fields govern crack development; toughness K_c , hardness H , and stiffness E then enter as basic material parameters in the fracture mechanics.^{1,2} Apart from their more direct uses in materials evaluation,^{1,3} sharp-contact indentation techniques have important applications in the fields of strength and strengthening,² erosion,⁴ and wear.^{5,6}

Cracks induced by elastic/plastic contact may be classified into two primary systems^{1,7}: those cracks which form on symmetry median planes containing the load axis and those which form laterally on planes closely parallel to the specimen surface. The present paper deals with the first of these, the "median/radial" system. Cracking of this type has long been recognized in the hardness testing of more brittle materials, by virtue of characteristic surface traces emanating radially from the impression corners. However, quantitative use was not made of such observations until Palmqvist demonstrated that the length of the radial cracks could be related empirically to toughness.⁸ Palmqvist worked exclusively with metal carbides, and his work accordingly received little attention in the ceramics literature.

A more fundamental approach to the median/radial problem, based on Griffith/Irwin fracture mechanics, has recently been developed.¹ Once the underlying indentation driving forces for the fracture have been identified and formulated, this approach provides the framework for a complete analysis of crack evolution; in particular, specific relations for crack dimensions as a function of contact load may be determined, with toughness K_c and other material parameters entering the description in a natural way. The first study along these lines was by Lawn and Swain,⁷ who considered the growth of subsurface median cracks within an essentially elastic point-contact field. Hardness entered the equations via the assumption that some plasticity would be necessary to remove stress singularities at the indenter tip. However, this initial attempt oversimplified the problem by using two-dimensional fracture mechanics to solve an essentially three-dimensional problem. A subsequent study⁹ took into account the observation that all well-developed cracks in point loading tend to penny-like geometry. While noting that residual stresses about the plastic zone must play some role in the crack evolution, particularly in the enhancement of surface radial extension during indenter unloading, the modified analysis retained the assumption that the primary crack driving force derived from the elastic field. Evans and Wilshaw¹⁰ took the analysis a step further by dealing with an elastic/plastic field from the outset and thereby maintained that the hardness-to-modulus ratio, H/E , should complement toughness as a controlling material parameter in the fracture mechanics. However, these workers used a semiempirical dimensional analysis to formulate their theory, thus avoiding a detailed description of the physical mechanisms responsible for fracture evolution. Evans and Wilshaw also extended the range of experimental observations, previously confined almost exclusively to the "model" material soda-lime glass, to polycrystalline ceramics. A principal finding here was a transition in the pattern of crack growth toward dominance of the surface radial component relative to the subsurface median in the earlier stages of loading as the ratio H/E diminished, notwithstanding the fact that the same, near-semicircular profile is almost invariably attained on removal of the indenter.

While these fracture mechanics investigations provided some indication of the role of plasticity in crack propagation, the only quantitative information came from strength-test procedures in which indentation methods were used to emplace starting flaws.¹¹ From these procedures it was found that toughness values evaluated from crack-size measurements were consistently smaller than those determined by independent means (typically by $\approx 30\%$). This discrepancy could be removed by polishing or annealing the indented test piece before breaking. It was therefore concluded that the newly formed plastic impression in a contact event must exert a residual opening force on the accompanying cracks. Marshall and Lawn¹² incorporated this effect into a more comprehensive indentation analysis, giving explicit recognition to elastic and residual terms in the stress-intensity formulation. The new analysis provided a quantitative explanation of the evolution of median cracks in glass and emphasized the importance of considering the fracture mechanics during *unloading* as well as loading of the indenter. Application of the results to strength analysis¹³ revealed the residual component of the indentation stress field to be an even more important factor in the growth of degrading flaws than had hitherto been suspected. How-

Received October 23, 1979; revised copy received January 7, 1980.

Supported by the U.S. Office of Naval Research and by the Australian Research Grants Committee.

*Member, the American Ceramic Society.

†At the time this work was done, B. R. Lawn was on study leave from the University of New South Wales.

‡Now with the Department of Materials Science and Engineering, University of California, Berkeley, California 94720.

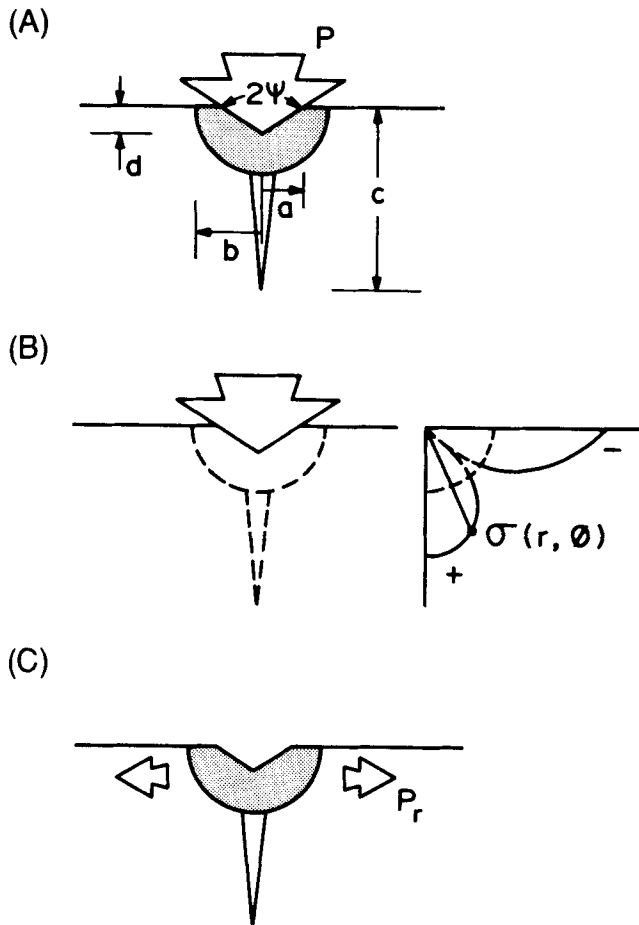


Fig. 1. Median/radial crack system, showing (A) elastic/plastic configuration at full load subdivided into (B) elastic component at full load plus (C) residual component at complete unload. In this model the indentation load P determines the intensity of the crack driving forces: the elastic component is characterized by the distribution of prior stresses $\sigma(r, \phi)$ normal to the crack plane (shown in (B) by stress contours in the median plane itself); the residual component is characterized by a residual center-opening force exerted by the radially expanded plastic zone.

ever, the approach adopted in this work was somewhat phenomenological, with certain indentation parameters in the fracture mechanics equations treated as adjustable constants to be determined empirically for any given indenter/specimen system. An immediate shortcoming of this approach is that observations of fracture evolution in one material are of little value in predicting the prospective performance of other materials; in particular, the theory offers no explanation of why median cracking appears dominant in some cases and radial cracking in others.

The objective of the present study was to reexamine, more critically, the elastic/plastic force field responsible for crack extension and thence to establish a rationale for predetermining the mechanics of the median/radial system for any material whose parameters K_c , H , and E are specified. Although it is acknowledged that the question of crack initiation can have an important bearing on the ensuing fracture geometry,¹ attention will be focused here on the propagation stage of crack development. Vickers indentations on soda-lime glass provide a reference indenter/specimen system for calibration purposes; the formulation is then shown to be capable of predicting all essential features of crack evolution in other selected materials. In the model developed here the role of the elastic component of the crack driving force is completely subordinate to that of the residual component.

II. Model of Median/Radial Crack System

All indentation fracture analyses begin with some knowledge of

the stress fields through which the cracks evolve.¹ If an exact solution for any given contact configuration is available it is possible, in principle, to determine the mechanics of crack development at all points of the loading cycle. However, the general complexity of elastic/plastic contact fields makes it necessary to introduce several simplifying approximations into the description. For instance, it is convenient to distinguish between the near and far fields about the deformation zone. The more complex question of crack initiation, so sensitive to the strongly inhomogeneous stress distributions about the elastic/plastic boundary, can then be separated out from the problem and the ensuing propagation accordingly treated without specific consideration given to details of contact.¹ While the initiation stage is certainly important in determining thresholds to fracture,¹⁴ and may well be a controlling factor in establishing the dominance of either a surface radial or subsurface median component in the earlier stages of propagation,^{15,16} the model developed here will pertain only to "well-developed" cracks. In this way it becomes possible to treat the median and radial extensions self-consistently in terms of a single-plane fracture system.

(1) The Basic Model

The major simplifying step in setting up the model is to subdivide the net indentation driving force for the fracture into well-defined components and then use the additive properties of stress intensity factors.¹⁷ This is done according to the scheme of Marshall and Lawn,¹² in which the elastic/plastic field of the fully loaded indenter is considered as the superposition of the residual field in the unloaded solid plus the field of an ideally elastic contact. Implicit in this scheme is the assumption that reversed plasticity does not occur during unloading of the indenter, a condition which should be satisfied to good approximation by the hard ceramic materials of special interest here.¹⁸

Figure 1 outlines the model. In (A) the indenter at load P generates a median-plane crack of characteristic dimension c . The plastic zone is taken to support the indenter, included angle 2ψ , over the characteristic contact dimension a , and to extend radially outward over a characteristic dimension b . Since the main concern is with crack propagation in the far field of the contact it is not necessary to specify the detailed geometry of the zone. The diagram shows only the downward dimension of the crack; however, the symbol c may be used to denote any polar dimension within the crack plane, most notably the surface radial and subsurface median dimensions c^R and c^M , respectively. It should also be borne in mind that a Vickers indenter will generally induce two mutually orthogonal median-plane crack systems of comparable dimensions.

Separation of the elastic/plastic problem into elastic and residual components is depicted in Figs. 1(B) and (C). The elastic field is taken to operate outside the plastic zone, i.e. in the region where cracking occurs,* reaching its maximum intensity of full loading and reversing completely on unloading. Because of this reversibility, the elastic driving force may be characterized by the stress distribution $\sigma(r, \phi)$ at $r \geq b$ (Fig. 1(B)) over the prospective crack plane¹⁷ and may therefore be obtained from classic elastic contact solutions. The residual field arises from mismatch tractions exerted on the surrounding matrix by deformed material within $r \leq b$; this component reaches maximum intensity at full loading but persists as the indenter is removed. In the approximation of well-developed cracks, i.e. $c \gg b$, these mismatch tractions manifest themselves as a net outward force acting at the crack center (Fig. 1(C)). It may be seen from Fig. 1 that adding configuration (B) to configuration (C) is equivalent to reloading the indenter to the original maximum load configuration (A).

(2) Stress Intensity Factors

In writing expressions for the stress intensity factors appropriate to the elastic and residual components of the composite elastic/plastic indentation crack system, Marshall and Lawn made use of two empirical observations¹²: (i) the indentation field satisfies the requirements of geometrical similitude, and (ii) the fully developed

*Microscopic observation of the radial cracks shows that fracture does not extend back into the deformation zone (Ref. 10).

median/radial fractures satisfy the relation $P/c^{3/2} = \text{constant}$ appropriate to center-loaded penny cracks. From these observations it was concluded that the stress intensity factors must both be of the form $K = \chi P/c^{3/2}$, with the χ terms constants to be determined for any given indenter/specimen system. It is pertinent now to examine this conclusion in terms of a more analytical treatment of the model in Fig. 1.

(A) *Residual Component*: Consider first the indented surface in the unloaded state (Fig. 1(C)). To evaluate the residual field component the following sequence of hypothetical operations is performed. (i) Begin with an *unstressed* elastic half space and remove a segment of material, characteristic radius b , from the prospective contact site. (ii) *Plastically* deform the removed segment by indentation over a contact a and penetration d , such that the irreversible strain associated with creation of the impression is accommodated by an expansion in characteristic zone dimension at constant volume of material. Then if δV is the volume of the impression and V is the volume of the zone, the configurational strain is of the functional form.*

$$\delta V/V \approx a^2 d/b^3 \approx (a/b)^3 \cot \psi \quad (1)$$

(iii) *Elastically* restore the segment to its original characteristic radius b by applying a hydrostatic compression across the outer boundaries,

$$p_b \approx \kappa (\delta V/V) \approx E (a/b)^3 \cot \psi \quad (2)$$

where κ is the bulk modulus and E the Young's modulus.† This pressure is to be distinguished from that which obtains at the impression at load P , i.e. the hardness,

$$p_a = P/\alpha_0 \alpha^2 \leq H \quad (3)$$

where α_0 is a geometrical indenter constant.‡ (iv) *Reinsert* the pressurized segment into the original cavity, restoring coherence at the interface, and allow the system to relax. It is clear from analogy with the internal spherical inclusion problem¹⁹ that the constraining pressure exerted on the relaxed segment will remain compressive but will reduce to some fraction of the pressure given in Eq. (2) (to one-half in an infinite matrix). Relaxation of the pressure over the surface diametral plane must inevitably modify the stresses at the elastic/plastic interface. Consequently, the plastic zone can be considered as a source of effective outward residual force on the crack shown in Fig. 1(C); the magnitude of this force may be obtained by integrating the horizontal stress components over the zone cross section within the crack plane, assuming p_b to remain effectively invariant with crack size.§

$$P_r \approx p_b b^2 \quad (4)$$

In the limit of well-developed cracks, $c \gg b$, the forces in Eq. (4) may be regarded as concentrated at a point. Assuming penny-like crack geometry, the stress intensity factor due to the residual far-field force may be written²⁰

$$K_r \approx f(\phi) P_r / c^{3/2} \quad (5)$$

where $f(\phi)$ is an angular function introduced to allow for the effects of the free surface; generally $f(\phi)$ is a slowly varying function, of value near unity, with its minimum at $\phi = 0$ (median orientation) and maximum at $\phi = \pm 90^\circ$ (radial orientation).²⁰ Equations (2) to (4) then combine with Eq. (5) to give

$$K_r = \chi_r P / c^{3/2} \quad (6)$$

with

$$\chi_r \approx f(\phi) (a/b) (E/H) \cot \psi \quad (7)$$

To take the analysis further it is necessary to specify how the ratio a/b varies with the indenter/specimen system. A detailed treatment of the analogous expanding cavity problem in an infinite isotropic elastic/plastic matrix gives the approximate result

$$b/a \approx (E/H)^m (\cot \psi)^{1/3} \quad (8)$$

where $m \approx 1/2$ (Appendix B). On the assumption that this result remains a good approximation for the equivalent half-space problem, substitution into Eq. (7) gives

$$\chi_r = \xi_r(\phi) (E/H)^{1-m} (\cot \psi)^{2/3} \quad (9)$$

where $\xi_r(\phi)$ is now a dimensionless term independent of the indenter/specimen system. In accordance with the median/radial dichotomy, the two quantities ξ_r^M and ξ_r^R (with $\xi_r^R > \xi_r^M > 0$) are of particular interest.

(B) *Elastic Component*: Now consider the contribution to the crack driving force from the elastic matrix itself (Fig. 1(B)). As indicated in Section II(1), this component can be evaluated in terms of the *prior* elastic contact stresses over the crack plane, at $r \geq b$. Since it is the far-field solution which is of concern here the stress distribution, at $r \gg a$, may be most conveniently represented by the point-load Boussinesq result⁷

$$\sigma(r, \phi) \approx g(\phi) P / r^2 \quad (10)$$

where $g(\phi)$ is another angular function; in this case $g(\phi)$ appropriate to stresses normal to the median plane is strongly varying, changing from positive (tensile) at $\phi = 0$ to negative (compressive) at $\phi = \pm 90^\circ$ (Fig. 1(B)). The stress intensity factor for a half-penny crack subjected to radially distributed stresses over $b \leq r \leq c$ is given by^{20,21}

$$K = f(\phi) (2/c)^{1/2} \int_b^c r \sigma(r) dr / (c^2 - r^2)^{1/2} \quad (11)$$

Ignoring effects due to the $g(\phi)$ functional variation for the present, Eq. (10) may be substituted into the integral to yield an elastic stress intensity factor of the familiar form

$$K_e = \chi_e P / c^{3/2} \quad (12)$$

where

$$\chi_e \approx f(\phi) g(\phi) \ln \{ (c/b) [1 + (1 - b^2/c^2)^{1/2}] \} \quad (13)$$

In the required limit $c \gg b$, Eq. (13) reduces to

$$\chi_e = \xi_e(\phi) \ln (2c/b) \quad (14)$$

where $\xi_e(\phi)$ is another global term. Again, ξ_e^M and ξ_e^R (with $\xi_e^M > 0$ and $\xi_e^R < 0$) are identified as key constants in the present analysis.

The parameter χ_e in Eq. (14) warrants further comment. First, it contains a logarithmic term in crack length, so the stress intensity factor in Eq. (12) is not strictly of the simple center-loaded penny form assumed in previous studies. On the other hand, over the typical range of indentation sizes encountered in the testing of ceramics, $1 < c/b < 10$, χ_e is not strongly varying. Second, in integrating the stress distribution over the prospective crack plane, improper allowance was made for variations along the ϕ coordinate: to regard $\xi_e(\phi)$ in Eq. (14) as being determined by the product $f(\phi)g(\phi)$ is a clear oversimplification. However, it will be argued later that K_e is secondary in importance to K_r in determining the ultimate crack configuration; in this light the approximations made in deriving Eq. (14) are not considered critical.

(3) Equilibrium Relations for Median and Radial Cracks

The condition for equilibrium growth of the cracks is obtained by equating the net stress intensity factor, K , to the toughness, K_c . For the system in Fig. 1 this condition is

$$K = K_e + K_r = K_c \quad (15)$$

*In the equations in this paper the double tilde (\approx) is used to indicate "varies as."

†Throughout this analysis, terms in Poisson's ratio will be neglected to avoid unnecessary complication. Empirical justification for this omission comes from the observation that "universal" curve fits to indentation data are insensitive to the relatively small variations in Poisson's ratio which occur in different ceramics (Ref. 3).

‡In this work, hardness is defined in terms of the *projected* rather than the *actual* area of contact. Thus, for pyramid indenters $\alpha_0 = 2$, which differs slightly from the value used in evaluating the conventional Vickers hardness number.

§This assumption has some experimental justification (Ref. 12). Theoretical analysis (Appendix A) does in fact show that the crack opening force P_r varies slowly with c .

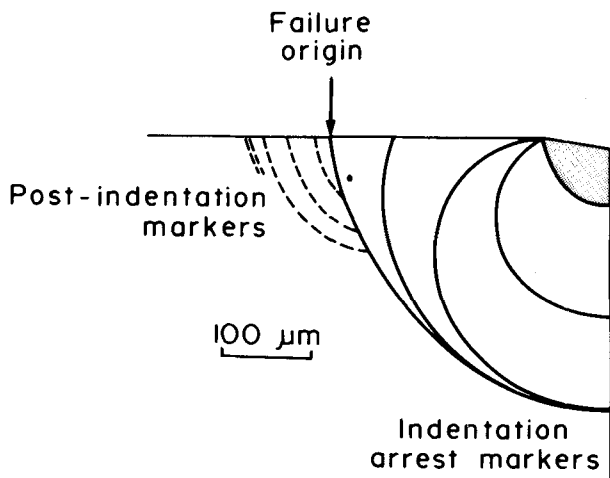


Fig. 2. Half-side view and half-schematic of median/radial crack system in soda-lime glass. Micrograph shows fracture surface of specimens broken at indentation sites; crack-arrest markings are introduced to provide record of crack evolution. Note failure origin at surface trace of half-penny.

Bearing in mind the reversibility of the elastic term, Eq. (12), and the irreversibility of the residual term, Eq. (6), separate equations may be written for the loading and unloading half-cycles¹²:

$$\chi_e P/c^{3/2} + \chi_r P/c^{3/2} = K_c \quad (P \uparrow) \quad (16a)$$

$$\chi_e P/c^{3/2} + \chi_r P_\star/c^{3/2} = K_c \quad (P \downarrow) \quad (16b)$$

where P_\star is the peak load. If the crack maintains a semicircular front throughout its evolution, it follows from Eq. (16) that the equilibrium radius at maximum load $P \uparrow = P_\star$ is

$$c_\star = [(\chi_e + \chi_r) P_\star / K_c]^{2/3} \quad (17a)$$

and correspondingly at complete unload $P \downarrow = 0$ is

$$c_\dagger = (\chi_r P_\star / K_c)^{2/3} \quad (17b)$$

However, two factors need consideration at this point. The first concerns the practical fracture conditions under which the requirements of mechanical equilibrium can be maintained. In particular, crack growth is not generally reversible, so Eq. (17b) cannot represent an attainable equilibrium configuration unless $c_\dagger > c_\star$. For the median component, $\chi_e^M > 0$, so the only way of realizing this inequality is somehow to suppress crack growth during the loading half-cycle (e.g. by superposing a reversible surface compressive stress).¹² For the radial component, on the other hand, $\chi_e^R < 0$, so the inequality is automatically satisfied. Thus the median crack is expected to attain its maximum growth during the loading half-cycle, whereas the radial crack is expected to continue its growth until unloading is complete.

The second factor concerns the angular variations inherent in the χ parameters. These angular variations are manifest in the identification of the median and radial crack components as separate entities in the evolution. Direct insertion of Eqs. (9) and (14) into Eq. (16) cannot therefore be expected to provide a highly accurate representation of the growth history at those stages where departures from radial symmetry within the crack plane are most apparent. Fortunately, the problem is minimal in the configuration which is ultimately of greatest concern, namely that at full unloading, where the tendency to ideal penny-like geometry is strongest.

III. Experimental Observations

The evolution of the median/radial crack system was monitored optically. For transparent materials, crack development could be followed during the indentation cycle, from either the side or below the specimen.^{10,12} Alternatively, a useful record of crack history could, in favorable cases, be reconstructed after indentation by examining fractographic features on specimens subsequently made to fail from one of the two mutually orthogonal half-pennies (Fig. 2).¹² In all cases the loading cycle was carried out in an inert environment (e.g. dry nitrogen gas or paraffin oil), to maintain near-equilibrium conditions in the crack growth, and with a Vickers

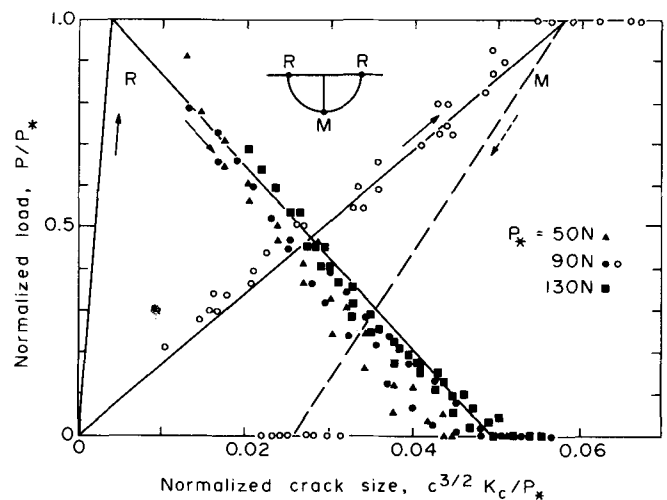


Fig. 3. Fracture mechanics plots for median and radial evolution in soda-lime glass, dry N_2 environment. Open symbols designate median cracks, filled symbols radial cracks (fractographic data, cf. Fig. 2). Solid lines are fits to Eq. (16). (Normalized impression size $a^{3/2} K_c / P_\star = 0.008$ at $P_\star = 50$ N, so that radial cracks "contained" within the contact zone during loading half-cycle for all P_\star values used.)

pyramid indenter to ensure reproducibility in the crack pattern.

Soda-lime glass, because of its transparency, isotropy, homogeneity, and general availability, was used as a reference material in the present study. Indentation-load/crack-size results, suitably normalized to produce linear, universal plots for all peak loads, are shown for median and radial components in Fig. 3; the data points represent experimental observations made on several cracks and the solid lines represent curve fits. Under normal test conditions, data could be obtained for medians only during the loading half-cycle and for radials only during the unloading half-cycle. The median data at $P \downarrow = 0$ in Fig. 3 were derived from a contrived test arrangement in which a reversible flexural stress was superimposed on the indentation field; this closure stress suppressed growth during loading to the extent that $c_\star^M < c_\dagger^M$ (Section II(3)), thereby producing a final equilibrium crack configuration equivalent to that which would have obtained under normal circumstances had healing been permissible.¹² Extension of the radial data to the loading half-cycle would have required loads in excess of the maximum used here, to enforce propagation of the expanding, subsurface crack to the free surface ("breakthrough").⁷ The indentation coefficients in Eq. (16) now follow directly from the slopes and intercepts of the fitted lines in Fig. 3: for the median component, $\chi_e^M = 0.032 \pm 0.008$ and $\chi_r^M = 0.02 \pm 0.003$ ¹²; for the radial component, $\chi_e^R = -0.045 \pm 0.002$ and $\chi_r^R = 0.049 \pm 0.004$.

The determination of reference coefficients in this way affords a useful "calibration" of the fracture mechanics equations for the

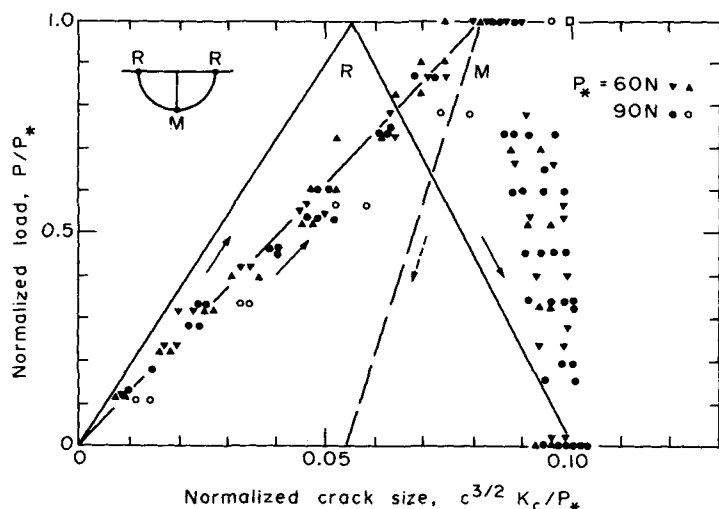


Fig. 4. Fracture mechanics plots for median and radial evolution in zinc sulfide, oil environment. Solid lines are predictions of calibrated Eq. (16); data points were obtained from direct observation of cracks through specimen wall.

median/radial system; predictions of crack evolution can now be made for any material of specified parameters K_c , H , and E . According to Eq. (14), the coefficients pertaining to the elastic component of the indentation field involve only spatial factors, in which case χ_e^M and χ_e^R should be the same for all materials.* The residual component, on the other hand, is seen from Eq. (9) to be material-sensitive; evaluation of χ_r^M and χ_r^R for different specimens accordingly requires specification of appropriate ξ_r terms in this equation. With the value of E/H for glass taken from Table I and $\psi = 74^\circ$ the characteristic half-angle for Vickers indenters, the values obtained are $\xi_r^M = 0.017 \pm 0.001$ and $\xi_r^R = 0.032 \pm 0.002$.

Indentation fracture data were collected for two other materials, zinc sulfide and silicon, to investigate the effect of changing E/H ratio. The results for zinc sulfide are shown in Fig. 4. This time the solid lines are a priori predictions from Eq. (16), using the preceding calibrated coefficients along with Eq. (9) and the material parameters in Table I. Of special interest here is the enhanced radial crack growth during the loading half-cycle in comparison with the glass results (Fig. 3). This follows directly from Eq. (17a): increasing E/H expands χ_r relative to χ_e , thereby "washing out" to some extent the strong angular factor inherent in the elastic coefficient (cf. Eqs. (9) and (14)). With silicon, measurements were made of the crack dimensions only at full load and full unload. Table II compares the measured dimensions with those predicted from Eq. (17), again using the calibrated coefficients. Notwithstanding certain discrepancies in the earlier stages of crack evolution, the theory appears to be consistent with the calibrated coefficients.

IV. Discussion

The fracture mechanics model presented here provides the framework for a quantitative analysis of the median/radial crack system in elastic/plastic indentation. Central to the analysis is the separation of the indentation force field into "elastic" and "residual" components, as characterized by the χ terms. For materials such as soda-lime glass at the high end of the hardness-to-modulus spectrum, i.e. approaching $H/E = 0.1$, these two components are of comparable magnitude. However, being reversible, the elastic driving force takes on a subordinate role in the crack evolution: whereas it does enhance crack growth in the subsurface median orientation, it serves merely as a restraining influence on the growth in the surface radial orientation. Moreover, since $\chi_r \approx (E/H)^{1-m}$, with $m \approx 1/2$, while χ_e remains effectively constant over the load range of practical indentation testing, the residual component becomes even more dominant as hardness-to-modulus diminishes. It is evident that deformation processes become a controlling factor in sharp-contact fracture.

*Actually, the elastic stress field does depend on Poisson's ratio (Ref. 7), the effects of which have been neglected here.

Table I. Parameters of Materials Studied

Material	Comment	E (GPa)	H (GPa)	K_c (MPa·m ^{1/2})*
Soda-lime glass	Amorphous	70	5.5	0.75
Silicon	Monocrystal	168	9	0.7
Zinc sulfide	Polycrystal	102	1.9	1.0

*Double-torsion data, dry N₂ environment.

Table II. Median and Radial Crack Data* for Silicon (111)

	Computed	Measured
$(c_{\star}^M)^{3/2} K_c/P_{\star}$	0.063	0.064 ± 0.004
$(c_{\star}^R)^{3/2} K_c/P_{\star}$.014	.031 ± 0.005
$(c_{\dagger}^R)^{3/2} K_c/P_{\star}$.059	.069 ± 0.006

*Fractographic data (cf. Fig. 3), $P_{\star} = 10\text{--}30$ N (13 cracks).

The fact that the radial crack configuration satisfies the requirements of mechanical equilibrium throughout the entire indentation cycle, approaching its final crack size on unloading, is of special significance in ceramics testing. Equation (17b) then applies, so that, in conjunction with Eq. (9),

$$c_{\dagger}^R = \{\xi_r^R (\cot \psi)^{2/3} [(E/H)^{1/2}/K_c]\}^{2/3} P_{\star}^{2/3} \quad (18)$$

This relation provides a physical basis for characterizing the indentation fracture from surface-trace measurements alone, an obvious advantage for opaque materials. It may be noted that while several indentation constants need to be specified in the description of full crack evolution, only one, ξ_r^R , enters in Eq. (18). It may also be noted that Eq. (18) is of the form $P/c^{3/2} = \text{constant}$ appropriate to penny cracks in ideal center loading: it is the appearance of the quantity E/H , in addition to the toughness K_c , which emerges as the primary manifestation of the elastic/plastic far-field driving force for the fracture.

The results embodied in Eq. (18) have important implications in two major areas of materials evaluation:

(A) *Toughness*: Previous studies, in recognizing that sharp-contact damage patterns contain explicit information on the relative susceptibilities of any given material to deformation and fracture, attempted to construct "universal" diagrams for quantifying mechanical response in terms of characteristic indentation dimensions.^{10,22} Evans and Charles²³ showed that such constructions may be used as a simple yet powerful means for determining the toughness of ceramics. These writers, working with materials whose K_c values had been measured independently, found it necessary to introduce an empirical correction factor in H/E to obtain a satisfac-

tory “calibration” of their universal plot. The present analysis serves to establish the Evans-Charles approach on a more fundamental footing, at least in the limit of the far-field approximation. Thus Eq. (18), in conjunction with Eq. (3) at $a = a_*$ and $P = P_*$, gives

$$(K_c H a_*^{1/2})(H/E)^{1/2} = 0.028 (c_r^R/a_*)^{-3/2} \quad (c_r^R \geq a_*) \quad (19)$$

using the previously cited values of α_0 , ψ , and ξ_r^R appropriate to Vickers indentations. This expression differs in form from that derived by Evans and Charles only in the exponent of H/E , which they set at 0.4 by curve-fitting. Figure 5 is a replot of their universal diagram in accordance with Eq. (19). Recalling that it is the residual field which determines the final length of the surface radial crack, it becomes imperative to ensure that indentation measurements are made under conditions of true equilibrium before attempting to evaluate toughness from Fig. 5; exposure of the newly formed fracture to a reactive environment may result in considerable extension by slow crack growth, in which case the value determined will be somewhat less than the true K_c .

(B) *Strength*: For any material which fails from a flaw introduced by elastic/plastic contact, the residual indentation driving force must be taken into account in the assessment of strength. Marshall *et al.*¹³ showed that this residual term could account for a strength reduction of $\approx 30\%$, consistent with the observations of earlier workers¹¹ (Section I). Working on the tacit assumption that failure occurs from the subsurface location $\phi = 0$, such that a relation of the form Eq. (17a) dictates the starting flaw size in the strength test, these writers also showed that for materials satisfying the inequality $\chi_r^M > \chi_e^M/3$ the cracks must undergo some precursor stable growth; i.e. failure is not spontaneous. This result was demonstrated to have important repercussions in the design of high-strength systems. In the present study, the conclusion that $\chi_r^R > \chi_r^M$ would suggest that failure is more likely to occur at a surface location $\phi = \pm 90^\circ$, in which case a relation of the form Eq. (17b) (more specifically, Eq. (18)) should determine the starting flaw size. The elastic parameter, χ_e^R , does not enter the analysis at all this time, so the condition for the existence of an energy barrier to failure is met automatically. Following the analysis by Marshall *et al.*¹³ the strength equation corresponding to flaws induced by indenters of given geometry takes the form

$$\sigma \approx (K_c^4/\chi_r)^{1/3}/P_*^{1/3} \approx [K_c^4(H/E)^{1/2}]^{1/3}/P_*^{1/3} \quad (20)$$

where Eq. (9) has been used to introduce the H/E dependence. This does not represent a serious modification to the earlier analysis¹³; the relation $\sigma P_*^{1/3} = \text{constant}$ still obtains for any given material and toughness remains the controlling material parameter.

In any applications of the indentation theory in areas such as those outlined it is necessary to be aware of some of the departures from the idealized system of Fig. 1 that can occur in practice. For instance, it has been assumed that material beneath the indenter deforms radially at constant volume. In materials with low values of H/E there is a tendency for displaced material to “pile up” around the indenter, approaching the “fully plastic” conditions exhibited by most soft metals.²⁴ Other, hard materials with “open” network structures, such as the “anomalous” silicate glasses, tend to accommodate the contact stresses by densification rather than by plastic flow.²⁵ In both of these cases the intensity of the residual driving force on any median/radial cracks must be substantially reduced. Comparative birefringence studies of indentation sites in normal vs anomalous glasses confirm this expected trend²⁶; indeed, the driving force for the median/radial system is diminished to such an extent in the anomalous glasses that Hertzian cone cracking becomes the dominant mode of fracture.^{25,26}

Another prospective complication that needs consideration is that of crack-interaction effects. It is implicit in the model developed in Section II that the median/radial crack system generates on a single, well-defined symmetry plane. The extent to which this picture represents a true crack configuration depends in part on the initiation history. For instance, with Vickers indentations at loads just above threshold, radial cracks may be seen emerging from just two, or three, corners¹⁶; clearly, development of cracking on one plane impedes development on a second, mutually orthogonal plane.

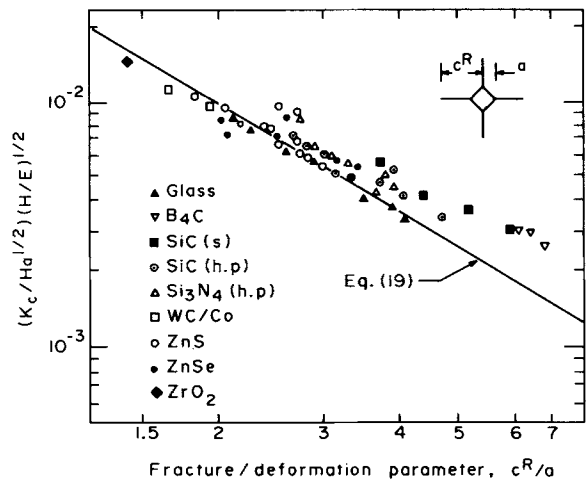


Fig. 5. “Universal” plot of radial crack data for toughness evaluation. Solid line is prediction of Eq. (19). ZnS and glass were tested in inert environment, other materials in air.

Also, where radial and median components initiate as separate entities, as they appear to do in zinc sulfide,¹⁰ coalescence into a single system may involve a step-formation mechanism where crack overlap occurs, thereby locally pinning the outward-expanding front. However, these disruptions are likely to become of secondary importance as an increasing load drives the cracks outward into a well-developed system.

More severe disruptions may occur in situations where alternative crack systems become unusually active during the indentation, thereby interfering directly with median/radial growth. Thus, in the case of the anomalous glasses dominant cone fracture provides confining boundaries for any surface radials or subsurface medians that may form.^{25–27} An analogous effect is also seen in “normal” soda-lime glass: Kirchner and Gruver²⁸ observed in impact experiments that the median-plane cracking occurs only in a shallow surface region at high target temperatures. Although this observation is commensurate with a transition from median-dominated to radial-dominated crack growth due to a diminishing ratio H/E as temperature increases, it is not immediately clear why the surface segments did not expand downward into the familiar half-penny configuration on unloading. However, Kirchner and Gruver also noted that the radial segments were accompanied by particularly large lateral cracks; the implication is that in this instance the expansion of the laterals preceded that of the radials, thus confining the surface crack. Provided due allowance is made for such geometrical variants, e.g. by a suitable recalibration of the basic fracture mechanics relations, the general applicability of the indentation method as a tool for materials evaluation remains intact.

One point not given explicit attention here, but which emerges in a natural way from the analysis, is the role of the characteristic indenter half-angle ψ as a variable in the fracture mechanics. From Eq. (18), for instance, it is seen that sharper indenters should give rise to larger cracks. However, care should be exercised in attempting absolute predictions concerning the effects of indenter geometry; issues such as elastic recovery of the residual impression and increased probability of pileup around sharper indenters have not been considered in the present analysis.

Finally, a comment on terminology may be appropriate here. The terms “median” and “radial” used to describe what is ostensibly a single-crack system have caused some confusion in the scientific literature. The model outlined provides a rationale for distinguishing between the two terms. It appears reasonable to suggest that “radial” be used in the description of any property which relates more closely to the surface dimensions of the crack pattern. The measurement of toughness and the analysis of strength in point contact, as discussed in this section, are cases in point. Conversely, “median” should be used when the crack depth is the controlling

dimension. Linear contact situations, e.g. glass cutting and particle abrasion, where the strength-determining crack remains subsurface, afford the best-known examples in this category.

APPENDIX A

Compliance Relations for Median/Radial Crack System

In Section II (1)(A) it was tacitly assumed that the residual crack-mouth opening force P_r (Fig. 1(C)) is independent of crack size c . In reality, because the compliance of the crack system must increase as fracture proceeds, the effective outward residual force exerted by the deformation zone must correspondingly relax.

This relaxation process may be conveniently represented in terms of a simple linear spring analog. According to the model of Fig. 1, the central deformation zone may be regarded as a precompressed spring inserted at the mouth of the crack system. The outward force exerted by such an element may be written as a function of wall displacement u_r ,

$$P_r/P_{r0} = 1 - u_r/u_{r0} \quad (\text{A-1})$$

where P_{r0} is the force in the fully compressed state (i.e. at $u_r=0$) and u_{r0} is the displacement in the fully relaxed state ($P_r=0$).

A compliance relation for the crack system, expressing P_r and u_r in terms of c , is now needed to facilitate evaluation of the required function $P_r(c)$. This relation may be obtained from the standard fracture mechanics equations¹⁷

$$G_r = K_r^2(1 - \nu^2)/E \\ = 1/2 P_r^2 dN/dC \quad (\text{A-2})$$

with G_r and K_r the crack extension force and stress intensity factor associated with the residual stress component; here $\lambda = u_r/P_r$ is the compliance in the approximation $c \gg b$ and $C = \pi c^2/2$ is the crack-plane area. Inserting Eq. (5) for the residual stress intensity factor (with $f(\phi)$ averaged over all ϕ taken as a proportionality constant β in this equation) into (A-2) and integrating gives the compliance relation

$$u_r/P_r = [2\pi(1 - \nu^2) \beta^2 b E] (1 - b/c) \quad (\text{A-3})$$

where a condition of zero compliance at $c=b$ is taken as an approximate boundary condition.

The displacement u_r may now be eliminated from Eqs. (A-1) and (A-3) to obtain

$$P_r = P_{r0} \{ 1 + [2\pi(1 - \nu^2) \beta^2 P_{r0} b E u_{r0}] (1 - b/c) \} \quad (\text{A-4})$$

This becomes a relatively slowly varying function of crack size in the far-field fracture region $c \gg b$. Consequently, P_r may be considered as effectively constant in Eq. (5).

APPENDIX B

Plastic Zone Characteristics: Expanding Cavity Analog

The analog of a spherical cavity under internal pressure is used here to relate the relative plastic zone radius b/a to the hardness-to-modulus ratio H/E and the indenter angle ψ .^{*} Evidence indicating that both the indentation pressure (hardness) and the plastic zone radius are reasonably well represented by this analogy resides in the results of two previous indentation studies. In the first, by Samuels and Mulhearn,³⁰ plastic zone observations can be interpreted to suggest that the plastic zone dimension is dictated by the volume of the indentation and, therefore (on the premise of constant plastic work), that the indentation pressure is insensitive to the indenter profile. In the second, by Marsh,³¹ the results demonstrate that, for a fixed-profile indenter, the variation of indentation pressure with

^{*}The approach adopted here differs from that proposed by Johnson (Ref. 29); his analysis is based on a model which allows the indentation pressure to be transmitted via an incompressible, hydrostatic core beneath the indenter.

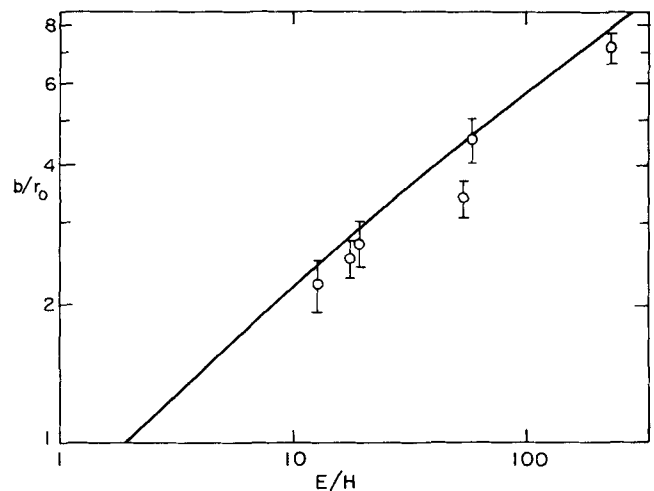


Fig. B-1. Plot showing expanding cavity relation (Eq. (B-1)) between hardness-to-modulus ratio and the ratio of plastic zone radius to cavity radius. Data points represent experimental measurements of plastic zone dimensions in (left to right) glass, $\text{Al}_2\text{O}_3\text{-ZrO}_2$, KCl, ZnS, cold-rolled steel, and hot-rolled brass (Ref. 32).

yield stress and elastic moduli closely resembles the predictions of Hill's elastic/plastic internal cavity analysis.¹⁸

Hill's analysis provides a relation for H/E in terms of the ratio of plastic zone radius to cavity radius:

$$H/E = (2/9)[1 + \ln(b/r_0)^3] \{ (1 - \nu)(b/r_0)^3 - 2(1 - 2\nu)/3 \} \quad (\text{B-1})$$

where r_0 is the cavity radius and b is the plastic zone radius. Equation B-1 is plotted, for $\nu=0.25$, in Fig. B-1. This function is nearly linear in logarithmic coordinates over a wide range of b/r_0 , so that a simple power law relation

$$b/r_0 \approx (E/H)^m \quad (\text{B-2})$$

where $m \approx 1/2$, affords a reasonable approximation. If we allow the volume of the cavity to equal the volume of the indentation, i.e. $r_0 = a[(\cot\psi)/\pi]^{1/3}$ for a pyramidal indenter, Eq. B-2 becomes

$$b/a \approx (E/H)^{1/2} (\cot\psi)^{1/3} \quad (\text{B-3})$$

Experimental measurements of plastic zone dimensions for six materials are plotted in Fig. B-1 (using the preceding relation between r_0 and a). The data are consistent with Eq. B-2. A more detailed correlation between the internal cavity analysis and experimental measurements of plastic zone dimensions and hardness will be reported later.³²

References

- B. R. Lawn and T. R. Wilshaw, "Indentation Fracture: Principles and Applications," *J. Mater. Sci.*, **10** [6] 1049–81 (1975).
- B. R. Lawn and D. B. Marshall; pp. 205–29 in *Fracture Mechanics of Ceramics*, Vol. 3, Edited by R. C. Bradt, D. P. H. Hasselman, and F. F. Lange. Plenum, New York, 1978.
- A. G. Evans, *Fracture Toughness: the Role of Indentation Techniques*. *Am. Soc. Test. Mater., Spec. Tech. Publ.*, **1980**, No. 678.
- A. G. Evans; pp. 303–31 in Ref. 2.
- M. V. Swain; pp. 257–72 in Ref. 2.
- J. D. B. Veldkamp, N. Hatt, and V. A. C. Snijders; pp. 273–301 in Ref. 2.
- B. R. Lawn and M. V. Swain, "Microfracture Beneath Point Indentations in Brittle Solids," *J. Mater. Sci.*, **10** [1] 113–22 (1975).
- S. Palmqvist, "Occurrence of Crack Formation During Vickers Indentation as a Measure of the Toughness of Hard Metals," *Arch. Eisenhuettenwes.*, **33** [9] 629–33 (1962).
- B. R. Lawn and E. R. Fuller, "Equilibrium Penny-Like Cracks in Indentation Fracture," *J. Mater. Sci.*, **10** [12] 2016–24 (1975).
- A. G. Evans and T. R. Wilshaw, "Quasi-Static Solid Particle Damage in Brittle Solids: I," *Acta Metall.*, **24** [10] 939–56 (1976).
- (a) N. Ingelstrom and N. Nordberg, "The Fracture Toughness of Cemented Tungsten Carbides," *Eng. Fract. Mech.*, **6** [3] 597–607 (1974).
(b) J. J. Petrovic, R. A. Dirks, L. A. Jacobson, and M. G. Mendiratta, "Effects of Residual Stresses on Fracture from Controlled Surface Flaws," *J. Am. Ceram. Soc.*, **59** [3–4] 177–78 (1976).
- D. B. Marshall and B. R. Lawn, "Residual Stress Effects in Sharp Contact Cracking: I," *J. Mater. Sci.*, **14** [8] 2001–12 (1979).
- D. B. Marshall, B. R. Lawn, and P. Chantikul, "Residual Stress Effects in Sharp Contact Cracking: II," *ibid.*, [9] 2225–35.

¹⁴B. R. Lawn and A. G. Evans, "A Model for Crack Initiation in Elastic/Plastic Indentation Fields," *ibid.*, **12** [11] 2195-99 (1977).

¹⁵C. M. Perrott, "Elastic/Plastic Indentation: Hardness and Fracture," *Wear*, **45** [2] 293-309 (1977).

¹⁶J. Lankford and D. L. Davidson, "The Crack Initiation Threshold in Ceramic Materials Subject to Elastic/Plastic Indentation," *J. Mater. Sci.*, **14** [7] 1662-68 (1979).

¹⁷B. R. Lawn and T. R. Wilshaw, *Fracture of Brittle Solids*; Ch. 3. Cambridge University Press, London, 1975.

¹⁸R. Hill, *The Mathematical Theory of Plasticity*; Ch. 5. Oxford University Press, London, 1950.

¹⁹J. D. Eshelby; pp. 89-140 in *Progress in Solid Mechanics*, Vol. 2. Edited by I. N. Sneddon and R. Hill. Wiley-Interscience, New York, 1961.

²⁰G. C. Sih, *Handbook of Stress Intensity Factors*. Lehigh University Press, Bethlehem, Pa., 1973.

²¹A. S. Kobayashi; pp. 4-37 in *Experimental Techniques in Fracture Mechanics*. Edited by A. S. Kobayashi. Iowa State University Press, Ames, Ia., 1973.

²²B. R. Lawn and D. B. Marshall, "Hardness, Toughness, and Brittleness: An Indentation Analysis," *J. Am. Ceram. Soc.*, **62** [7-8] 347-50 (1979).

²³A. G. Evans and E. A. Charles, "Fracture Toughness Determinations by Indenta-

tion," *ibid.*, **59** [7-8] 371-72 (1976).

²⁴D. Tabor, *Hardness of Metals*. Clarendon Press, Oxford, 1951.

²⁵J. T. Hagan, "Cone Cracks Around Vickers Indentations in Fused Silica Glass," *J. Mater. Sci.*, **14** [2] 462-66 (1979).

²⁶A. Arora, D. B. Marshall, B. R. Lawn, and M. V. Swain, "Indentation Deformation/Fracture of Normal and Anomalous Glasses," *J. Non-Cryst. Solids*, **31** [3] 415-28 (1979).

²⁷P. Chantikul, D. B. Marshall, B. R. Lawn, and M. G. Drexhage, "Contact-Damage Resistance of Partially Leached Glasses," *J. Am. Ceram. Soc.*, **62** [11-12] 551-55 (1979).

²⁸H. P. Kirchner and R. M. Gruver; pp. 365-77 in Ref. 2.

²⁹K. L. Johnson, "The Correlation of Indentation Experiments," *J. Mech. Phys. Solids*, **18** [2] 115-26 (1970).

³⁰L. E. Samuels and T. O. Mulhearn, "An Experimental Investigation of the Deformed Zone Associated with Indentation Hardness Impressions," *ibid.*, **5** [2] 125-34 (1957).

³¹D. M. Marsh, "Plastic Flow in Glass," *Proc. R. Soc. London, Sect. A*, **279**, 420-35 (1964).

³²S. S. Chiang, A. G. Evans, and D. B. Marshall, "Indentation Response of Solids"; unpublished work.

Effect of Thermal Expansion Mismatch on the Thermal Diffusivity of Glass-Ni Composites

BOB R. POWELL, Jr.*

Department of Materials Science and Engineering, University of California, Berkeley, California 94720

G. E. YOUNGBLOOD*

Montana Energy and MHD Research and Development Institute, Butte, Montana 59701

D. P. H. HASSELMAN* and LARRY D. BENTSEN*

Department of Materials Engineering, Virginia Polytechnic Institute and State University, Blacksburg, Virginia 24061

The effect of interfacial decohesion, due to the thermal expansion mismatch, on the thermal diffusivity of a hot-pressed glass matrix with a dispersed phase of nickel was investigated by the laser-flash technique at 25° to 600°C. The interfacial gap formed on cooling acts as a barrier to heat flow and lowers the thermal diffusivity to values below those predicted from composite theory and also creates a strongly positive temperature dependence of the thermal diffusivity. Preoxidation of the Ni spheres promotes interfacial bonding and yields values of thermal diffusivity higher than those for nonoxidized spheres and a thermal diffusivity which is relatively temperature-independent. The results of the present study also confirm the criteria for the effective thermal diffusivity of composites established by Lee and Taylor.

I. Introduction

MANY composite materials have been developed to meet the special requirements for many engineering applications. Such composites frequently exhibit favorable properties not found in the individual components. The science of "composite theory"

for calculating the properties of composites from the properties of the components represents a very active field.

For calculating the thermal conductivity of composites for a wide variety of phase compositions and distributions, many expressions are available from the literature.¹⁻⁴ These theories, however, generally assume that perfect bonding exists between the components. For this reason, the interfacial boundaries offer no resistance to the transport of heat through the composite. In practice, however, many composites will exhibit less than perfect bonding between the components as the direct result of poor wettability or the absence of good mechanical adhesion. This problem is expected to be especially severe for composites with a large mismatch in the coefficients of thermal expansion of the components. Changes in temperature of such composites can lead to the formation of high values of "internal" stress, which can lead to "microcracking" of the components or to interfacial separation, depending on the direction of the mismatch. Such microcracking can also occur in polycrystalline materials which exhibit a high degree of thermal expansion anisotropy of the individual grains. In these latter materials microcracking results in major decreases in the thermal diffusivity,^{5,6} in accordance with analytical results for the effect of cracks on thermal conductivity.⁷ Similar effects would be expected for composites with a large mismatch in thermal expansion. However, as far as the present writers are aware no such experimental data exist in the literature.

The purpose of the present study was to investigate the effect of the mismatch in thermal expansion on the thermal diffusivity of a bonded and nonbonded composite consisting of a low thermal

Received October 29, 1979; revised copy received February 19, 1980.

Supported by the Office of Naval Research under Contract Nos. N-00014-78-C-0726 and N-00014-78-C-0431.

*Member, the American Ceramic Society.

*Now with General Motors Research Laboratories, Warren, Michigan 48090.